LAWRENCE
LIVERMORE
NATIONAL
LABORATORY

UCRL-TR-230646

RadTracker: Optical Imaging of High Energy Radiation Tracks

S. P. Vernon, M. E. Lowry, B. J. Comaskey, J. E. Heebner, J. S. Kallman, J. B. Richards

May 2, 2007

Disclaimer

This work performed under the auspices of the U.S. Department of Energy by Lawrence Livermore National Laboratory under Contract DE-AC52-07NA27344.

FY06 LDRD Final Report
RadTracker: Optical Imaging of High Energy Radiation Tracks
LDRD Project Tracking Code: 05-ERD-058

Stephen P. Vernon, Principal Investigator

Abstract

This project examined the possibility of extending the recently demonstrated radoptic detection approach to gamma imaging. Model simulations of the light scattering process predicted that expected signal levels were small and likely below the detection limit of large area, room-temperature detectors. A series of experiments using pulsed x-ray excitation, modulated gamma excitation and optical pump-probe methods confirmed those theoretical predictions. At present the technique does not appear to provide a viable approach to volumetric radiation detection; however, in principal, orders of magnitude improvement in the SNR can result by using designer materials to concentrate and localize the radiation-absorption induced charge, simultaneously confining the optical mode to increase "fill" factor and overlap of the probe beam with the affected regions, and employing high speed gated imaging detectors to measure the scattered signal.

Introduction

This work was focused on exploring the development of a new type of imaging gamma detector that could allow an observer to detect the location of a gamma emitting source, with very high efficiency, and large standoff. The approach relies upon newly developed optical techniques for radiation detection.

Recently, we predicted and demonstrated[i] a new radiation detection mechanism which we have called the radoptic effect. It is well-known that when ionizing radiation is absorbed by a semiconductor, e-h pairs are produced. Researchers in nonlinear optics have used optical beams to produce e-h pairs in semiconductors, which in turn produce a change in the material's index of refraction as measured by an optical probe beam. Linking these two processes, the radoptic effect is the use of ionizing radiation to produce a similar change in the index of refraction. An optical probe beam is then passed through the region of perturbed index. The probe beam is phase-modulated by the presence of the index perturbation. This phase-modulation is then measured and related to the ionizing radiation fluence.

Our first generation of detectors used interferometric techniques to measure the optical phase modulation and thus obtain a measurement of the impinging xray radiation. In the development of our 2nd generation of radoptic detectors[ii], we used cavity-based interferometry and established that we could detect a single xray photon. An interesting result from this earlier work is that these detectors are sensitive to the radiation flux per

unit area, not to radiation flux. In other words, given a spatially uniform radiation intensity, if you increase the area of the detector, the optical signal you detect does not increase in amplitude. Another way of looking at that result is that with these detection mechanisms, you get spatial resolution for free—smaller detector areas do not decrease the signal level. This earlier detector work focused on high temporal resolution and high spatial resolution for xrays. As a result, they tended to be relatively small devices with characteristic dimensions of microns.

While leveraging this early high-sensitivity detector work, the present work explores how large the detection area can be while also achieving very good single-particle detection sensitivity—specifically for gamma radiation. Detecting gammas with high probability also requires "thick" detectors to accommodate the gammas long interaction lengths. Thus the detectors for this work are very large volume devices, ultimately on the order of several cm^3. A Compton gamma detector using the radoptic effect is illustrated in figure 1. The Compton effect produces two regions in space with perturbed e-h pair density — thus producing two "tracks" which are optical phase objects. The first phase object is produced at the location where the incoming gamma is scattered; the scattering event produces a Compton electron and a down-scattered Compton gamma that subsequently interacts with the material producing the second phase object. Analysis of the energy and momentum allows one to generate a "directionality cone" which describes the possible directions from which that incoming gamma entered the detector volume. Analysis of multiple events leads to intersecting cones, which can then be used to describe a unique incoming ray direction, and thus the direction of the gamma source from the observer. We call this approach RadTracker.

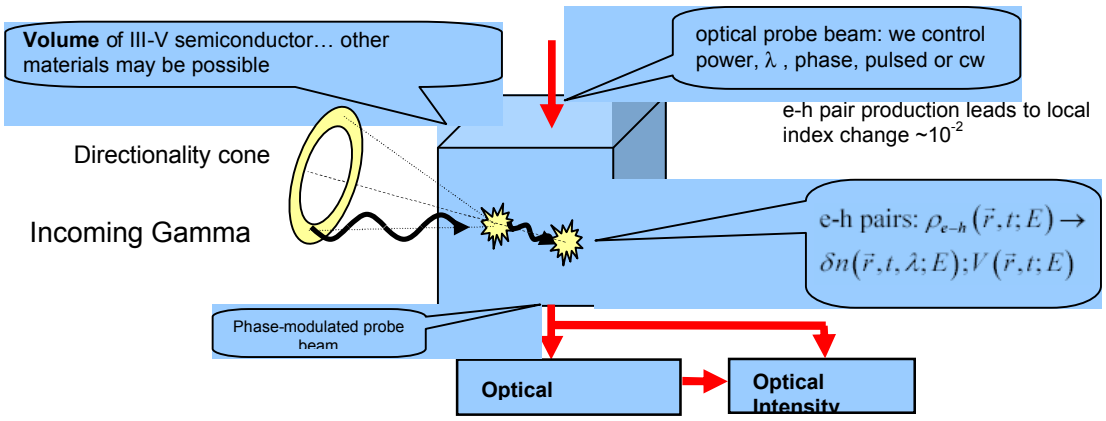

Figure 1. Block-diagram of a radoptic Compton effect gamma detector, RadTracker

Theoretical Background

In this section we develop and analyze a theory of operation for the optical detection mechanism of the RadTracker. The theory we develop here is an analytic scattering theory, however we have also performed numerical simulations using the beam propagation method and Mie scattering. This analytic theory and the numerical

simulations agree to within a few percent, so we will only discuss the analytic results, here, since they better illuminate the physics and limiting principles.

The number of electron-hole pairs produced by the absorption of ionizing radiation is initially given by[iii],

$$N_{eh0} = \frac{E_{\text{rad}}}{\frac{14}{5}E_{\text{g}} + E'} \qquad (1)$$

here E_{rad} is the energy deposited by the ionizing radiation particle, E_{g} is the semiconductor bandgap, and E' is an empirically derived constant, that is approximately 0.75 eV for GaAs, for instance. However, the number of carriers produced begins to decay through recombination, given by,

$$N_{eh} = N_{eh0}e^{-t/\tau} \qquad (2)$$

Also, the carriers begin to diffuse away from their initially small volume (high density), so the density, temporal and spatial evolution is given by,

$$\rho(x,y,z,t) = \frac{N_{eh}}{\pi^{3/2}w(t)^3}e^{-\frac{x^2+y^2+z^2}{w(t)^2}} \qquad (3)$$

Where $w(t) = \sqrt{w_0^2 + 4Dt}$; this results from solution of the isotropic diffusion equation assuming a Gaussian charge density of initial width w_0, and a diffusion constant, D.

This density of e-h pairs gives rise to an optical index change. We consider the two strongest mechanisms: exciton bleaching and free carrier absorption. In the case of exciton bleaching the index change is given by[iv],

$$\delta n(x,y,z,t) = CG(\lambda)F\left(\rho(x,y,z,t)\right) \qquad (4)$$

Where $F(\rho) = \frac{\rho}{\rho + \rho_{\text{sat}}}$, $G(\lambda) = \frac{\Gamma}{1+\Gamma^2}$, and $\Gamma = \frac{\lambda_g - \lambda}{\delta\lambda}$.

When $\rho << \rho_{\text{sat}}$, the index change can be written

$$\delta n(x,y,z,t) \approx \frac{CG(\lambda)}{\rho_{\text{sat}}}\rho(x,y,z,t) \equiv \frac{1}{\rho_{\text{R}}}\rho(x,y,z,t) \qquad (5)$$

We note that this condition on charge density is satisfied for most times, due to diffusion. For the case of free carrier absorption, we can write the index change as

$$\delta n(x,y,z,t) = \text{Re}\left\{\sqrt{1+\Delta\chi} - 1\right\} \approx \tfrac{1}{2}\Delta\chi_{\text{real}} = -\frac{e^2\rho(x,y,z,t)}{2m\varepsilon_0\omega^2} \equiv \frac{1}{\rho_{\text{R}}}\rho(x,y,z,t) \qquad (6)$$

This index perturbation produces a phase shift in an optical probe beam; for a probe beam propagating in the z direction the phase shift is calculate integrating the index change along the propagation direction, this gives

$$\Phi(x,y,t) = \int dz \ \frac{2\pi}{\lambda}\ \delta n(x,y,z,t) = \int dz \ \frac{2\pi}{\lambda}\ \frac{1}{\rho_R}\ \rho(x,y,z,t) = \frac{1}{\rho_R}\ \rho(x,y,t)\frac{2\pi\ \sqrt{\pi}w(t)}{\lambda} \equiv \delta\hat{n}(x,y,t)\ \frac{2\pi\ \sqrt{\pi}w(t)}{\lambda} \tag{7}$$

Where we have used Eq. (3), and $\rho(x,y,t) \equiv \frac{N_{eh}}{\pi^{3/2}w(t)^2} e^{\frac{x^2+y^2}{w(t)^2}}$

Inspection of these equations reveals that the optical phase shift is proportional to the incoming ionizing radiation particle energy.

We detect this spatially dependent phase shift by applying a collimated probe beam to a volume of detector material and measuring the light scattered by the radiation-induced phase object. A diagram of one experimental implementation is shown in figure 2.

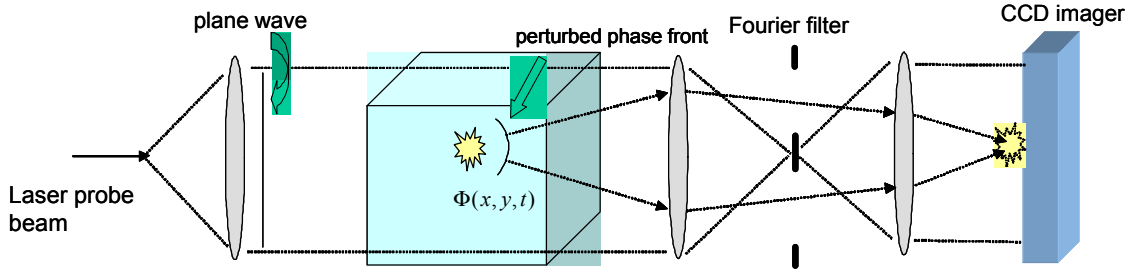

Figure 2. Imaging detection of optical scatter from an index perturbation

Fourier optics techniques are employed to block un-scattered light; collimated light appears at the center of the Fourier plane. By allowing the filter stop to have a non-zero transmission, we can also interfere some of the carrier with the scattered light on the CCD imager, enhancing the SNR in some cases.

If we assume that the incident intensity of the probe beam is I_0, and a, is the transmission of the filter stop, it can be shown that[v] the scattered intensity $I_s(x,y,t)$, is given by

$$I_s(x,y,t) = I_0\left(a^2 + 2a\Phi(x,y,t) + \Phi^2(x,y,t)\right).$$

The case of *a=0,* is often called dark-field imaging, otherwise it is called Zernike imaging.

We can then calculate the signal level, e.g. the number of detected, scattered photons from a single phase object, as

$$S_{rad} = \frac{\eta}{h\nu}\int_{A,t} dAdtI_s(x,y,t) = \frac{\eta}{h\nu}\int_t P_s(t)dt$$

Where we are integrating over the effective cross-sectional area of the phase object, and over its lifetime; $P_s(t)$ is the scattered optical power as a function of time, and η, is the quantum efficiency of the detector.

We note that the scattering signal from multiple radiation induced phase objects would be the sum of signals from individual isolated phase objects, as long as the phase objects were distinct and coherence effects can be ignored.

We can now plug in estimated values for all the parameters in the model and calculate $P_s(t)$. This result is shown in figure 3, where we show the predicted scattered power in watts, for 3 values of the diffusion constant, D (cm^2/s). For this calculation we have used the material parameters of GaAs, and

$E_{\text{rad}} = 2MeV$

$I_0 = 100kW/cm^2$

$w_0 = 0.1\ \mu\text{m}$

$C = 0.85$

$\rho_{sat} = 1.2x10^{18}\ \text{cm}^{-3}$

$\lambda = 920\ \text{nm}$

η=1

a=0; dark-field imaging

Integrating over time for the D=2 cm^2/s[vi] case this leads to $S_{rad} = 2.7$ detected photons for each 2Mev gamma. To first order, the signal level scales linearly with the number of gammas.

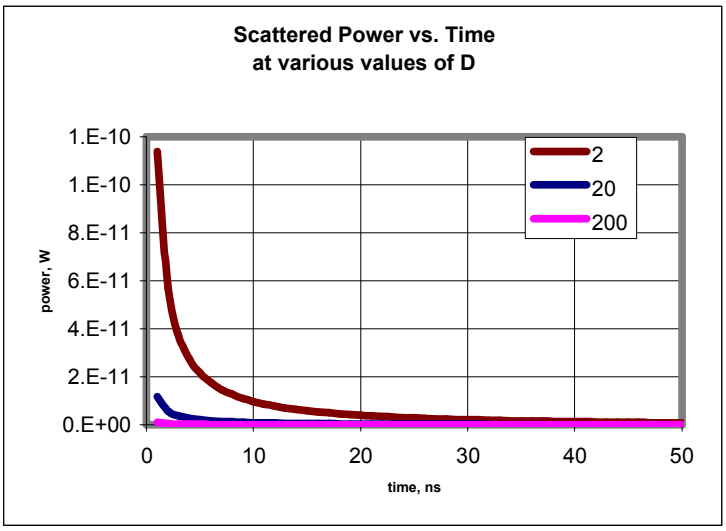

Figure 3. Scattered optical power versus time, for various values of D (cm^2/s)

The numbers make it clear that this will be a challenging signal to detect. To make matters even more difficult, there will be a background optical signal *B*, given by

$$B = \eta \int_{\hat{A},t} dAdtI_0(a^2 + \varepsilon)$$

Here ε is the scattered fraction of the incident radiation due to background scatter from defects and sources other than the radiation induces phase object, and the area of integration $\hat{A}$, is the size of the detector (pixel),. In this model the SNR of the detection system is,

$$SNR = \frac{S_{rad}}{\sqrt{S_{rad} + B + N_{readout}^2}}$$

Unfortunately, for our experiments we were restricted to using a relatively large area detector. A large detector area increases the value of B, and decreases the SNR. The situation could be improved somewhat by using more sophisticated gated imager detection, which would reduce the detector area for each pixel and decrease B; however, this complexity was beyond the scope of this exploratory work.

Experiments

Three excitation sources were employed in an attempt to measure these effects: pulsed x-ray excitation with 40 keV xrays, temporally modulated gamma irradiation (sealed ^{60}Co radiation source), and optical excitation using short pulse lasers.

Pulsed x-ray excitation

Our initial experiments aimed at measuring optical scatter using high energy, x-ray radiation from a Scandiflash unit. Figure 4 below includes a schematic and a photograph of the experimental arrangement. The Scandiflash was operated at 40 kV with a fill of 270 kPa of SF_6 and 290 kPa of dry air. The GaAs samples were located 21 cm from the

exit face of the x-ray tube and the initial experiments employed an integrating detector (photodiode) rather than a CCD imager. X-ray diodes (XRD) were used to monitor the x-ray flux and dosimiters placed at 30 and 37.5 cm from the x-ray tube were used to calibrate the diode signals. A typical shot yielded dosimeter readings of 35-40 mR. The light source was a 100 mW, diode-laser operating at 980 nm.

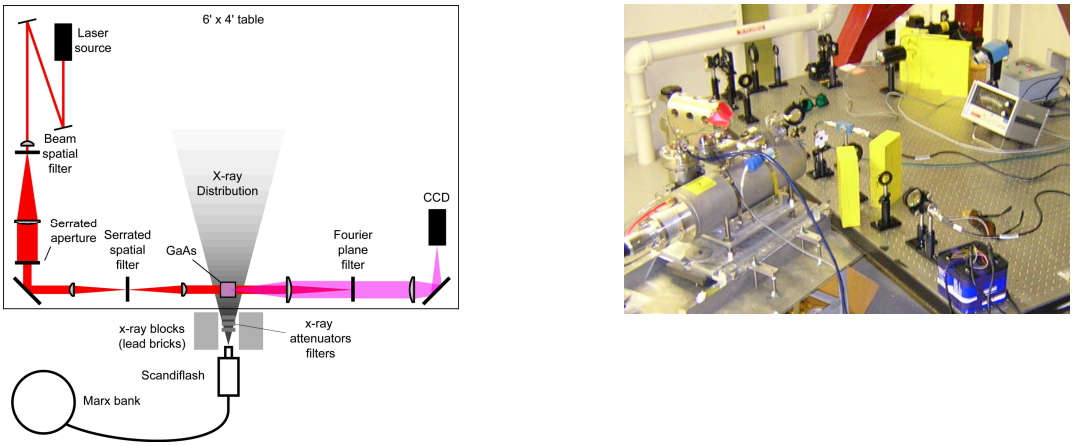

Figure 4. The experimental arrangement used for Scandiflash measurements

Figure 5 shows the difference in photodiode signals (red curve) for measurements made with and without incident laser light, and the XRD signals for sequential Scandiflash shots (blue, green). As illustrated in the figure the XRD signals for the two shots are comparable; however, the detector signal is dominated by electromagnetic interference (EMI) effects.

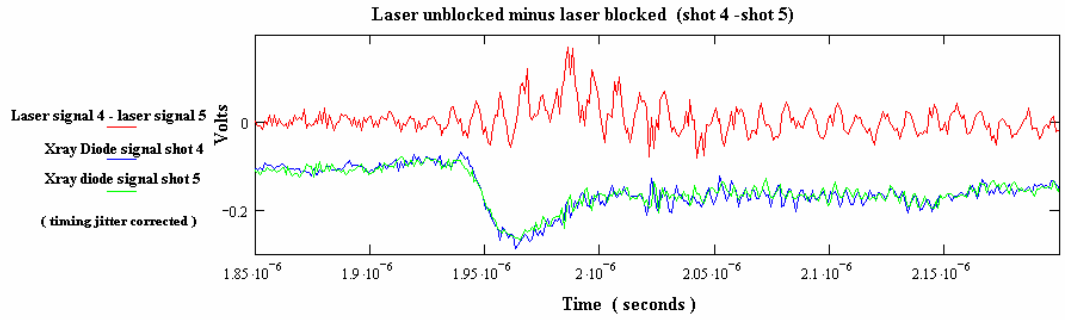

Figure 5. Difference in detector signals with and without laser illumination of the sample (red) and x-ray diode signals (blue, green). The detector signal is dominated by EMI.

In an attempt to minimize EMI pickup, we elected to employ a lens and optical fiber relay to transmit the scattered laser light to a remote recording alcove. This minimized the EMI signal but revealed an additional detection challenge that is illustrated in Figure 6. The upper panel shows the detected signal when the GaAs sample was illuminated with the laser and exposed to the x-ray pulse. The lower panel shows the detected signal when the sample was illuminated with the laser but the sample was shielded from the x-

ray output. The signals are self-similar and appear to result from an electro-optical effect related to the firing of the x-ray source; the signal does not depend upon x-ray irradiation of the sample. The middle panels illustrate the detected signals when the sample was exposed to the x-ray flux with the laser off and a situation where the laser was on but the sample removed.

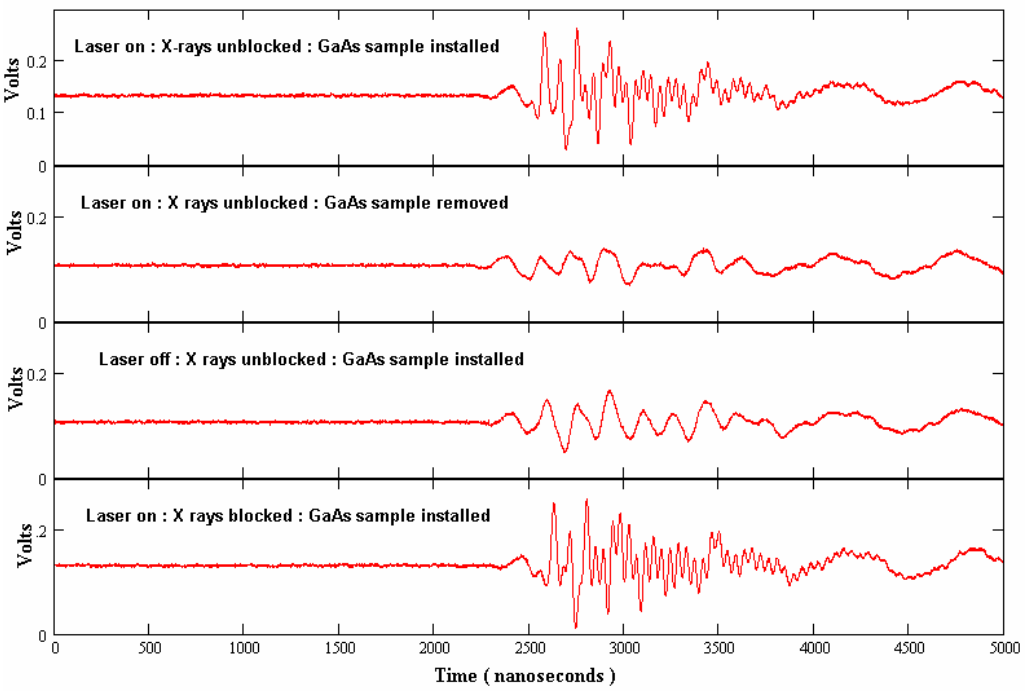

Figure 6. The experimental arrangement used for Scandiflash measurements

Modulated ^{60}Co sealed gamma source

We elected to circumvent the problem by abandoning the pulsed x-ray source in favor of using a sealed, 11.2 mC, ^{60}Co radiation source to irradiate the sample with ~1 MeV gamma radiation. The source provides an incident gamma flux of order 10^6/cm^2-sec at source distances of ~ 6 cm. Modulating the radiation flux via a mechanical chopper would admit the possibility of employing phase sensitive detection techniques and greatly increase the SNR as compared to single transient measurements.

The experimental arrangement is illustrated in figure 7. Modulation of the x-ray flux is accomplished using a mechanical chopper and the laser radiation is spatially filtered to block the CW beam and collect the scattered laser light. The detection system consisted of a Thorlabs PDA 550 amplified photodetector connected to the signal channel of an SRS Model 850 lock in amplifier using second harmonic detection. IR radiation reflected from the rotating chopper shaft and detected with a photodiode provided the reference signal for the lock-in amplifier. The laser source was a Toptica DL100 tunable diode laser system, in the Littrow configuration, operating at 930 nm.

At the outset we experimentally determined the sensitivity of, and stray light rejection requirements for, the detection system. The output laser beam was split into two arms:

CW laser light in the first arm was used to simulate the stray-light background; light in the second arm was modulated, using a mechanical chopper, to simulate the light

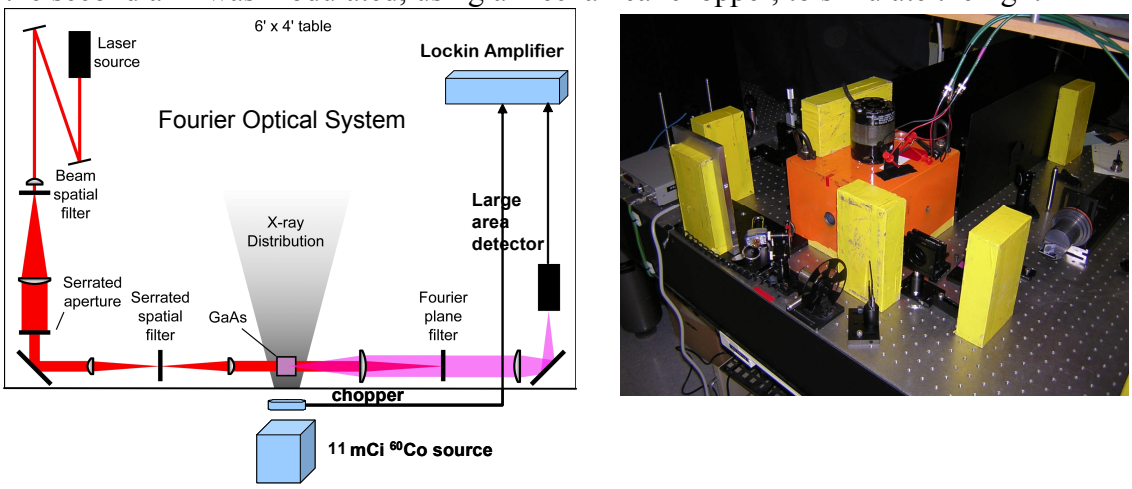

Figure 7. The experimental arrangement employed using the sealed ^{60}Co source. The orange cube in the photograph is the custom made Pb shielded enclosure that surrounds the modulated source.

scattering signal. Light from each arm was independently attenuated using ND filters and superimposed at the photodetector to derive the minimum detectable signal, and the stray light-level producing saturation, at a given detection sensitivity. In this configuration, the minimum detectable signal level was 10^{-13} Watts; in order to operate the detection system at this sensitivity, the DC level had to be maintained below 30 nW. For a CW laser power of 100 mW, this required a stray light rejection ratio of ~ 75 db.

Our baseline optical system design is shown in figure 8 and comprises a dark field imaging system. The laser is incident from the left. Lenses L1, L2 provide spatial filtering of the incident laser beam. L3 focuses un-scattered laser light onto the stop and, in combination with L4 creates a relay image of phase objects within the sample onto an image plane. All of our experiments employed large area integrating detectors.

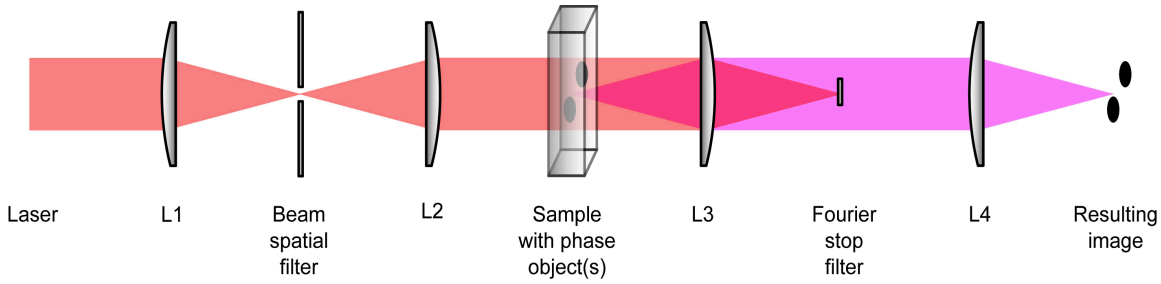

Figure 8. Design of the dark-field detection system. L1-L4 are AR coated achromats with f =150 mm

The optical design illustrated in figure 8, in principal, provides good rejection of the un-scattered laser beam; however, scatter from the optical surfaces can contribute to the detected signal. For example, scatter from L2 is not blocked by the stop and is imaged at the surface of L4; further, light scattered form the stop is re-scattered by L3 and the partially transmitted portion is re-scattered upstream. In practice we found that we could

not achieve the required 75 dB of stray light rejection with this design and adopted the geometry illustrated in figure 9; here we have attempted to minimize the number of surfaces in the optical path and have eliminated the optical stop, sacrificing collection solid angle.

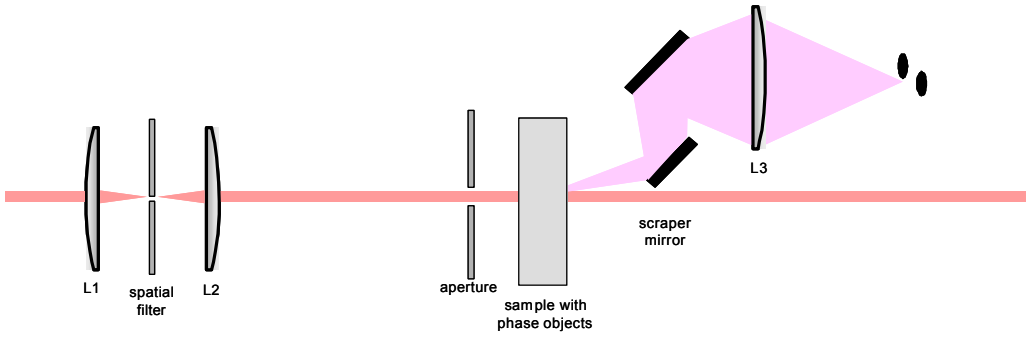

Figure 9. Detection configuration that minimizes the number of scattering surfaces in the beam path. This compromises detection sensitivity, in comparison to the arrangement illustrated in Fig 94, by reducing collection solid angle.

The model predictions of the viability of this approach were not promising – simulations indicated that we should expect a detection efficiency of order 10^{-5} (one scattered photon for every 100,000 incident gamma rays), the radiation source provided ~ 10^4 gamma/chopper period producing 0.1 scattered photons per chopper period, well below our measured detection sensitivity of 10^4 photons/chopper period. However, the model simulations depended, in detail, on parameters that are not well known. We therefore resolved to attempt the measurement fully aware of the challenges. No above-background signals were detected.

Optical Pumping

Our final experiments attempted to measure the light scattering signature using pump-probe optical techniques. Figure 10 shows a schematic of the experimental arrangement.

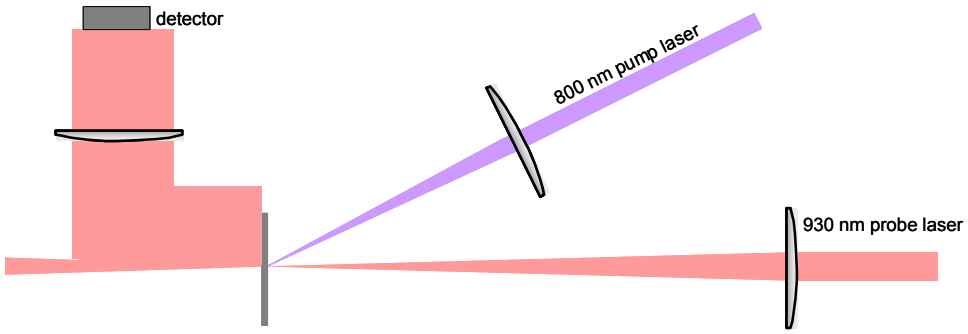

Figure 10. Experimental arrangement for pump-probe measurements

A Ti:sapphire pump laser (~140 fs pulse length, 1 kHz repetition rate @ 800 nm) provided above-band-gap optical excitation of the GaAs sample. The 930 nm probe laser was focused onto the sample surface and positioned to overlap the 800 nm beam. A portion of the scattered signal was intercepted by a pickoff mirror and focused through a band pass filter onto an amplified detector and recorded with an oscilloscope. At the sample surface the diameter of the 800 nm beam was ~ 60 μm; the diameter of the 930 nm beam spot was ~ 130 μm. In this arrangement no detectable signal was observed until the pump fluence was raised above the laser damage threshold of the sample (see Appendix A).

Conclusions

This project from its inception was the kind of high-risk, high-payoff effort that is uniquely suited to LDRD funding. Unfortunately, the optical signal levels were too small to be detected with our existing experimental setup. However, our analysis reveals several fundamental and interesting reasons:

1. The spatial extent of an individual phase-object is small compared to the volume being interrogated, this leads to severely degraded SNR when using large area detectors
2. The phase-shift over that local region for the material systems investigated is small, again degrading SNR
3. We should not ignore the interactions of multiple radiation induced phase objects. Our scattering model assumes a collection of isolated, distinct, spatially localized phase objects, in which the scattered light from multiple phase objects sums incoherently. However, in practice, after analyzing these results, it seems quite likely that two of our experimental setups (the xray scandiflash and optical pump setups), may not have yielded isolated phase objects. Rather, due to the high pump photon intensities (xrays in the first case, and optical photons in the second experiments) what we have is a very large collection of phase objects that are relatively close together spatially. Through diffusion, the size of the individual phase objects grows and the index contrast decreases. Furthermore, if you consider the effects of our probe beam passing through many layers of these relatively indistinct phase objects as it propagates along the z-direction, what starts out as a spatially inhomogeneous (in x and y) phase shift becomes homogenized as the probe beam wavefront encounters more phase shifts at randomly varying x,y locations. Thus, as the probe beam propagates through a sample of many "layers" the accumulated phase shift becomes spatially uniform. The effects of these interactions between phase objects on the total scattering needs to be analyzed more carefully theoretically, but it seems this may significantly decrease the scattering.

Item 3 presents an interesting dilemma. We had focused on pulsed experiments in an effort to maximize the number of phase-objects produced. It turns out that this may not have been the correct approach. There may be an optimum density of phase objects (or,

correspondingly, an optimum radiation flux) that will produce a maximum optical scattering.

These efforts did not achieve our goal of measuring the radiation induced optical scattering. As is the case with much research in new areas it has led us in unexpected directions and has resulted in a much better understanding of the physical process and yielded new ideas that may ultimately lead to the success of approaches like RadTracker.

Future Directions

Our initial experimental attempts led us to consider several ways in which the signal could be enhanced sufficiently to be detected. There are several approaches, we enumerate them in correspondence to our numbered conclusions

1. Increase the SNR using gated imagers. Our schematic in figure 2 depicts a CCD imager to be used as a detector. However, our experiments were limited to using a single large-area detector. If we had a high-speed, gated imager, we could dramatically increase the SNR, because now all of the scattered light will appear on only a few pixels and the amount of background light will be scaled as the ratio of the signal area to the entire CCD array area. Thus, to first order, the background noise could be reduced by $x10^6$.

2. Increase the SNR using "designer" materials and structures.
    a. The use of band-gap engineering to concentrate the electron-hole pairs, as illustrated in figure 11 can markedly increase SNR. This would allow the charge carriers to be collected by and concentrated within quantum well structures that simultaneously act as planar optical waveguides. The optical beam is confined within a planar waveguide that contains a high concentration of charge, if a radiation interaction occurs within that material slab. We estimate that we could use this technique to improve the SNR by at least a factor of 100. This will also reduce the laser power requirements by at least 100x.

    b. Materials with longer e-h lifetimes and lower diffusion constants could be sought to improve signal levels.

3. Finally, we note that any future experiments should be preceded by a more rigorous theoretical analysis of the effective interaction of multiple phase objects. This could lead to an optimum radiation flux for pulsed experiments, and thus, an optimized path towards experimental measurement of the scattering per absorbed ionizing radiation particle.

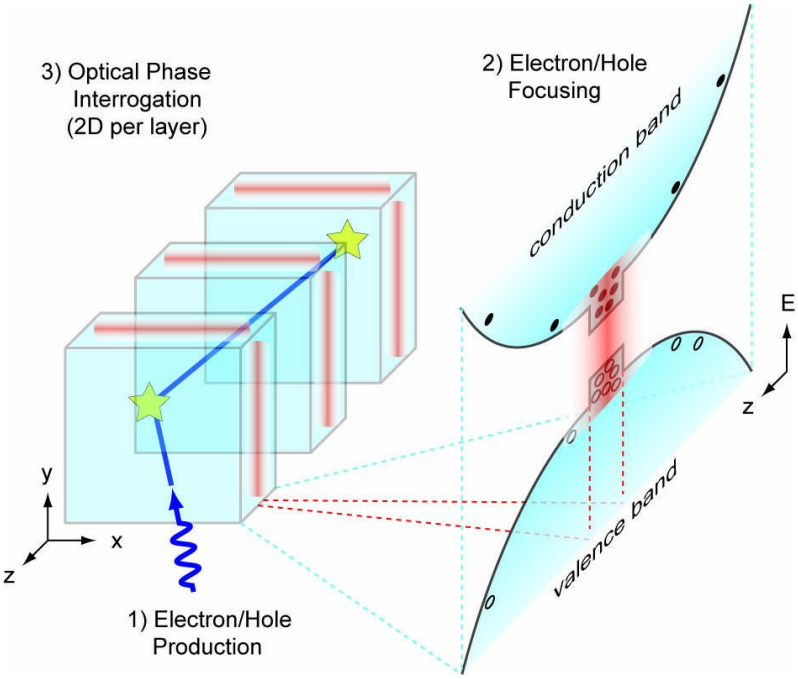

Figure 11. Tailored bandgap structures can simultaneously provide optical confinement and charge concentration yielding greatly enhanced SNR.

Appendix A

This appendix documents some of our observations on optical absorption induced changes to optical scatter in laser damaged GaAs. Study of these phenomena was beyond the scope of this LDRD project; however, the experimental observations mimicked some of the experimental signatures that we were seeking and, initially, confused the interpretation of the pump-probe experiments.

At the onset of laser damage in GaAs, a light scattering signal is observed with the following characteristics:

1. the signal is only observed when both beams (pump and probe) were present,
2. the integrated intensity of the signal is proportional to the pump power,
3. the amplitude and sign of the scattered signal is a function of position relative to the centroid of the damaged site
4. the signal is long-lived, with a characteristic decay time ~ 100 μs.

Figure A1, shows an optical micrograph of a damage site on a GaAs wafer produced by laser irradiation at a fluence slightly above the GaAs laser damage threshold.

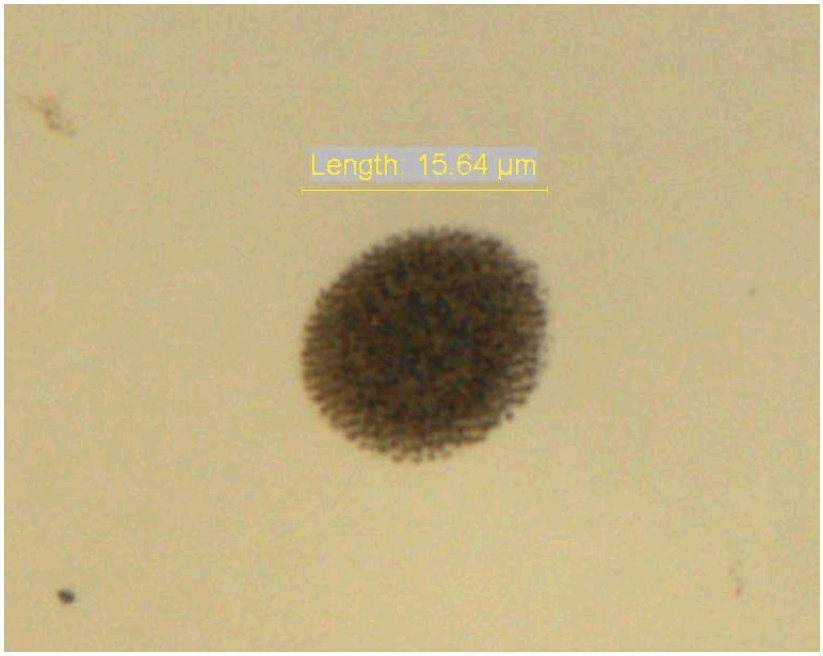

Figure A1.Optical micrograph of a laser damaged region of a GaAs wafer

Figure A2 illustrates the observed variation of the scattering signal with relative pump power after inducing laser damage to the sample. Figure A3 shows the dependence of

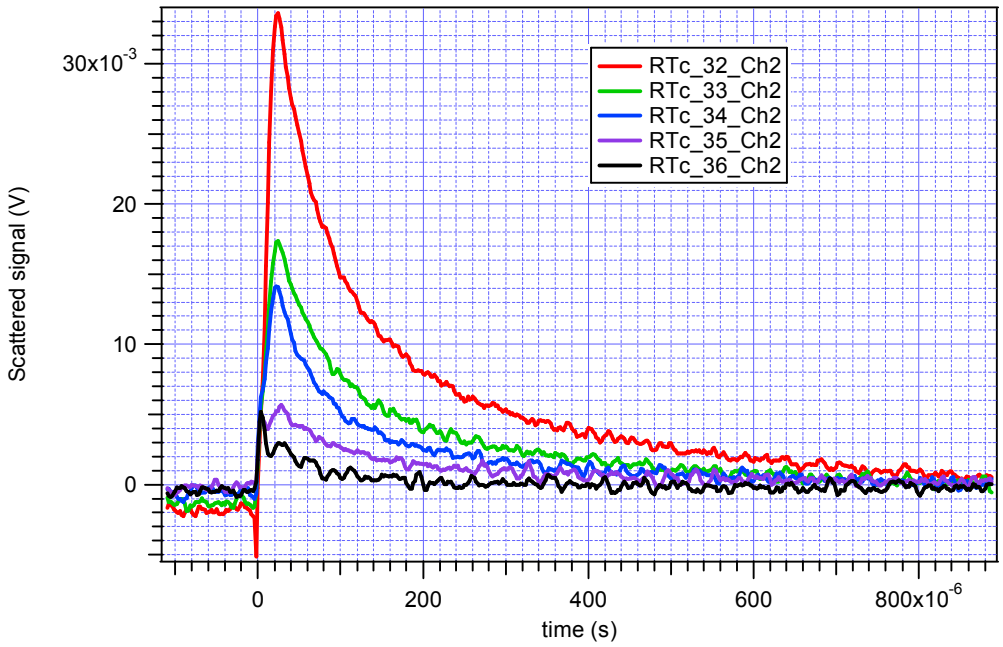

Figure A2. Detector voltage vs. time for increasing pump power: minimum power(black), maximum pump power (red).

integrated scatter on pump laser power. Measured points correspond to the normalized time integral of the curve traces in Figure A2.

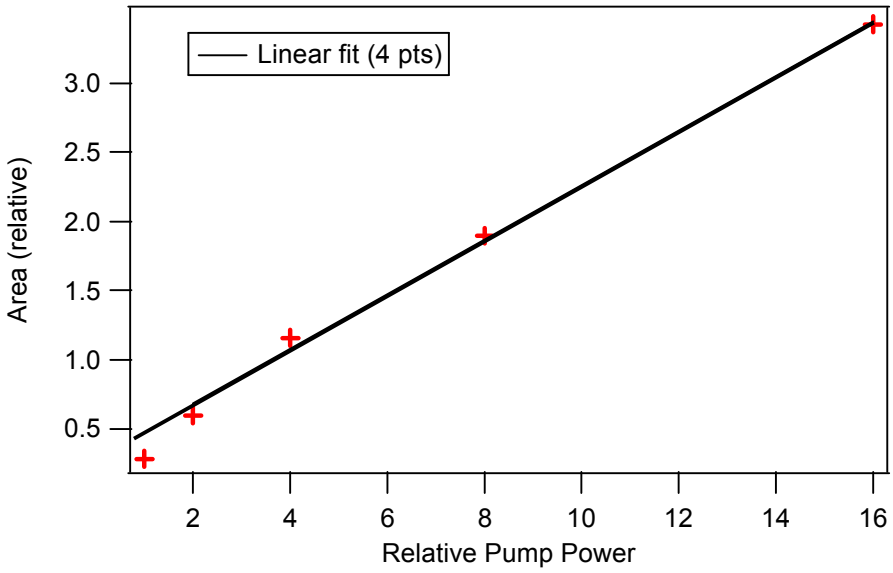

Figure A3. Variation of total integrated scatter with laser pump power.

Once the sample is damaged, the induced light scattering signal is a marked function of position of the pump and probe beams relative to the centroid of the damage site. This is illustrated in Figure A4 where we show scattered intensity vs. time for three positions on

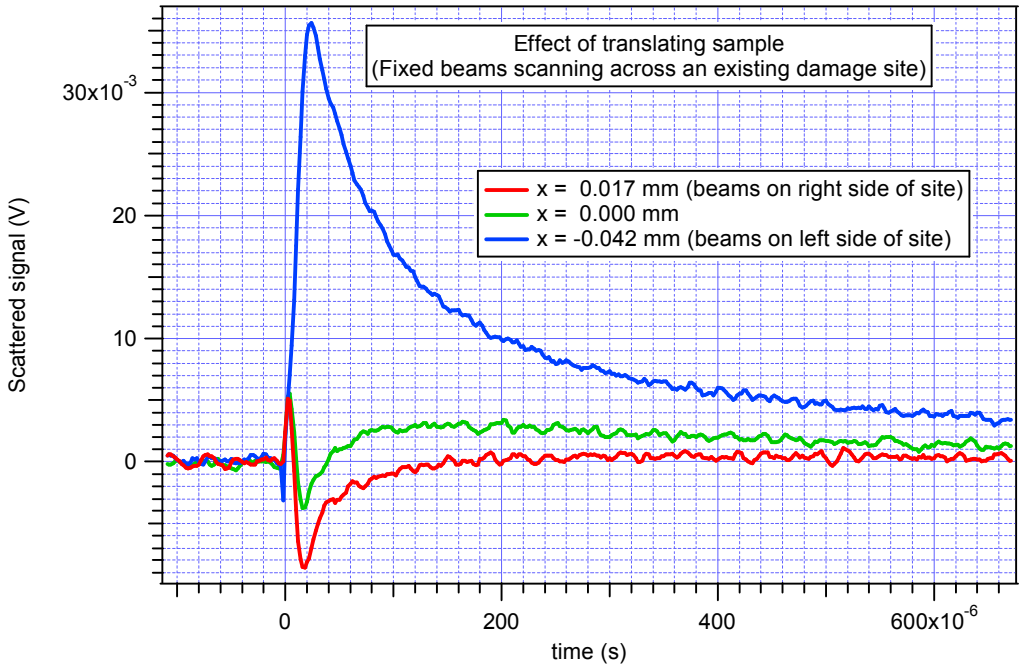

Figure A4. Scattered signal as a function of position relative to the damage site (x=0).

the wafer surface. After damage the sample was translated 17 μm, and with the pump beam fixed, the probe laser beam was translated across the surface to maximize the detected signal. After this initial optimization subsequent measurements were made by translating the sample.

References

[i] M. Lowry, et. al. "RadSensor: Xray Detection by Direct Modulation of an Optical Probe Beam", Paper #5194B-35, SPIE's 48th Annual Meeting, August 3-8, San Diego, CA (UCRL-243189)

[ii] M.E. Lowry, et.al. Rev. Sci. Instrum, vol. 75, #10, pp. 3995-97 (2004)

[iii] pg. 256, "Optical Processes in Semiconductors", Jacques I. Pankove, Dover, New York (1971)

[iv] Park, et.al., Appl. Phys. Lett. Vol. 52, pg1201 (1988)

[v] Born and Wolf

[vi] The lower diffusion constant seems most likely, since the diffusion "constant" is actually a function of charge density, higher charge density (our case here) decreases the diffusion constant. However, this aspect requires further analysis and experimentation to complete our understanding.